Properties of giant dipole resonances within an extended pairing model with a focus on spectral statistics

A. J. Majarshin ®,[1,2,3,*] Yan-An Luo,[1] Feng Pan,[2,4] H. Sabri,[3] M. Rezaei,[3] and Jerry P. Draayer ®[4]

[1]*School of Physics, Nankai University, Tianjin 300071, People's Republic of China*
[2]*Department of Physics, Liaoning Normal University, Dalian 116029, People's Republic of China*
[3]*Department of Physics, University of Tabriz, Tabriz 51664, Iran*
[4]*Department of Physics and Astronomy, Louisiana State University, Baton Rouge, Louisiana 70803-4001, USA*

In this paper, we report on a study of the spectral features associated with dipole resonances in medium-mass nuclei ($E \leqslant 12$ MeV), as revealed in the framework of the *spd*-interacting boson model. The effect of pairing correlations on the theory follows from solutions obtained through an application of the Bethe ansatz equation. In general, calculated spectra around the critical point of the vibrational to γ-soft transitions appear to approach those of a Gaussian orthogonal ensemble, while near the rotational and vibrational limits of the theory the spectra show more regular behavior. Specifically, the results reveal that the statistical features of the spectra are sensitive to the vector boson pairing strength c_p in the transition region; that is, when c_p is zero, or when the system approaches one of its dynamical symmetry limits, the spectra display regular features, while for stronger c_p values, or when near to the critical phase transition region, the spectral features show more chaotic behavior. Overall, our results indicate that the statistical features are governed by the interplay between dipole resonant energies, pairing correlations, and interactions between and among the single and vector boson modes of the theory. As part of this work we also found out that chaoticity occurred when results were fit to a Berry-Robnik distribution. Throughout our analyses, we used experimentally known information about both positive- and negative-parity states. Our findings suggest that dipole resonances appear to be best-described by Poisson statistics for $A \approx 32$–138 nuclei.

I. INTRODUCTION

High-resolution photonuclear experiments have been used for many years to explore special features of nuclear structure. Most recently they have been used to examine spectral statistics of dipole resonances, which in turn has provided a unique opportunity to investigate physical realizations of Gaussian orthogonal ensembles (GOEs) and Poisson distributions. These special features, as understood within the general framework of the random matrix theory (RMT) [1–3], can, in turn, be used to decipher whether a system displays chaotic or regular behavior by comparing the nearest-neighbor spacing distribution (NNSD) to Poisson and Wigner [1–5] distributions, respectively. In this paper, building forward on the work of Maino *et al.* [6] on the *spd*-interacting boson approximation (IBA) model, we use an extended version of the theory to study dipole resonances. Properties of giant dipole resonances (GDRs) have also been explored by other authors [7–10]. Specifically, resonances of this type have also been examined using Hartree-Fock-Bogoliubov approaches [11], the random phase approximation [12,13], and various other IBA-based theories [6,14–27].

The IBA, as proposed by Arima and Iachello, includes two types of bosons with angular momentum $L = 0$ (s bosons) and $L = 2$ (d bosons) [28–30]. Building forward from this, and following the work of Maino *et al.* [6,17], in this paper we consider the spectral statistics of GDR with an apparent BRD. Specifically, the scope of the present work is to describe dipole spectra by coupling a p boson to the IBA *sd*-boson system for a theory with three pairing control parameters (c_s, c_d, and c_p) and study the spectral statistics of the resultant high-lying dipole states. A focus on dipole states within such a framework started with the initial work of Morrison and Weise in 1982 [16] and, independently, the work of Scholtz and Hahne in 1983 [21] Subsequently, Rowe and Iachello in 1983 [8] proposed analytic results by extension of the IBA for energies and transition matrix elements. Maino *et al.* [6,17,23,25,27] have advanced such investigation from different points of view, such as dipole resonances in the light and odd-even nuclei. Recently, other authors have proffered that the presence of vibrational and low-lying rotational modes coupled to high-lying giant resonances in nuclei could be studied within the (*spd*-IBA) [8,16,21,31].

This integration of the IBA and GDR modes—especially for transitional nuclei—has also been discussed in Refs. [6,14,16,18–27]. An important additional advantage of using a mixed-mode *spd*-IBA system of this type is that it allows one to re-examine resultant level spacings in terms

*jalili@nankai.edu.cn; jalili@tabrizu.ac.ir

of their regularity and/or chaoticity. Accordingly, in what follows we report on results for ground and excited states of dipole resonances within this framework. In short, we find different degrees of chaoticity with a variation in the pairing strength by performing finite-size scaling up to $N = 10$ bosons.

Our approach is distinct from others that build directly on the work of Iachello and co-workers ([29,30,32–35]). Specifically, we utilize exact solutions of the IBA as advanced by Pan and co-workers [36–42], and further, we use an affine SU(1,1) algebraic technique to determine the properties of nuclei in the $U(5) \otimes U(3) \rightarrow SO(9)$ transitional region of the IBA. The latter requires the Hamiltonian be diagonalized numerically, as in Refs. [36,43–45].

The remainder of this paper is organized as follows. In Sec. II (Theoretical Framework), the dipole mode's coupling to the *sd*-boson model is expressed within the SU(1,1) framework. Section III (Numerical Results) focuses on comparisons with exact results in the *spd*-IBA for different sets of parameters. Also, to describe the NNSD, all level sequences of dipole resonance are prepared from the pairing model and classified based on their pairing strength. Sec. IV (Summary and Conclusion) is a brief recap of essential results.

II. THEORETICAL FRAMEWORK

The problem of missing levels hampers most statistical analyses of nuclear data. To address this issue, we analyze dipole states within the framework of an extended *spd*-IBA theory, where a comprehensive analysis of the GDR uses IBA methodologies for same-parity states and a dual-pairing-mode construction as realized through a SU(1,1) Lie algebra construction for opposite-parity configurations. We tested this methodology for a *spdf* - system [46] by analyzing the affine SU(1,1) Lie algebra within an IBA framework, focusing on low-lying dipole and octupole strengths. The results of that study suggested that some properties of GDR in collective states could be used as indicators of chaos and/or regularity in the mass region of shape phase transitions. If we restrict ourselves to a study of positive-parity and low-lying collective states, *s* and *d* bosons are sufficient for a complete accounting of spectra excitations (no missing levels), and at the same time, within this framework, the *sd*-IBA can account for collective monopole and quadrupole modes. The present work is focused on the spectral statistics of *p* bosons and GDR structures.

In recent years, the use of the Richardson model [47,48] has gained prominence, and extensions to it based on the use of the Bethe ansatz have been advanced [49,50]. For these infinite-dimensional algebraic Bethe ansatz approaches, the pairing Hamiltonian solutions are provided through a set of highly nonlinear Bethe ansatz equations (BAEs) [51–53]. By exploiting a dual algebraic structure [54,55] for a multilevel pairing model within an affine SU(1,1) Lie algebra, we can generate exact solutions of the three-level (*spd*-IBA) model for eigenvalues of dipole resonances in the transitional region of medium-mass nuclei. And in addition, we can use the *spd*-IBA to determine level spacings and their statistical behavior. So, in summary, in this paper we report on the results of

an application of the algebraic Bethe ansatz method, within the framework of an infinite-dimensional SU(1,1) Lie algebra [36,39], to generate the spectra of the dipole states and use the results to examine the statistical behavior (chaotic and regular) of the dipole states so generated.

spd model

To investigate the properties of GDR, similar to that of the two-level system in the *spd*-boson system, a three-level system in the *s*, *p*, and *d* boson model is considered here. To analyze the Quantum Phase Transition (QPT) between the spherical and rotational shapes, similar to Refs. [36,39], the SU(1,1) pairing algebra is produced by $S^\rho(l)$, $\rho = 0$ and $\pm$, which satisfies the following commutation relations:

$$[S_{(l)}^+, S_{(l)}^-] = -2S_{(l)}^0, \quad [S_{(l)}^0, S_{(l)}^\pm] = \pm S_{(l)}^\pm, \quad (1)$$

where l represents *s*, *p*, and *d* bosons with the angular momentum of 0, 1, and 2, respectively.

The creation operators of SU(1,1) quasi-spin pairing algebras for *s*, *p*, and *d* bosons are

$$S_s^+ = (S_s^-)^\dagger = \frac{1}{2}s^{\dagger 2},$$

$$S_s^0 = \frac{1}{4}(s^\dagger \cdot s + s \cdot s^\dagger) = \frac{1}{2}n_s + \frac{1}{4}, \quad (2)$$

$$S_p^+ = (S_p^-)^\dagger = \frac{1}{2}p^\dagger \cdot p,$$

$$S_p^0 = \frac{1}{4}\sum_\lambda (p_\lambda^\dagger \cdot p_\lambda + p_\lambda \cdot p_\lambda^\dagger) = \frac{1}{2}n_p + \frac{3}{4}, \quad (3)$$

$$S_d^+ = (S_d^-)^\dagger = \frac{1}{2}d^\dagger \cdot d,$$

$$S_d^0 = \frac{1}{4}\sum_\lambda (d_\lambda^\dagger \cdot d_\lambda + d_\lambda \cdot d_\lambda^\dagger) = \frac{1}{2}n_d + \frac{5}{4}, \quad (4)$$

where n_s, n_p, and n_d are the number operators for *s*, *p*, and *d* bosons.

The Casimir operator of SU(1,1) for each *l* boson can be expressed as

$$\hat{C}_2[SU(1,1)] = S^0(l)[S^0(l) - 1] - S^+(l)S^-(l). \quad (5)$$

The basis states of an irreducible representation of SU(1,1), $|\kappa\mu\rangle$ for *spd*-IBA, are determined by a single positive real number, κ, where $\mu = \kappa, \kappa + 1, \ldots$

Therefore,

$$\hat{C}_2[SU(1,1)]|\kappa\mu\rangle = \kappa(\kappa - 1)|\kappa\mu\rangle, \quad S^0|\kappa\mu\rangle = \mu|\kappa\mu\rangle. \quad (6)$$

Because the basis vector of $U(2l + 1) \supset O(2l + 1) \supset O(3)$ is simultaneously the basis vector of $SU(1,1)^l \supset U(1)_s^l$, their complementary relation can be expressed as

$$|N; n\nu LM\rangle = \left| N, \kappa^l = \frac{1}{2}\nu + \frac{1}{4}(2l + 1), \right.$$

$$\left. \mu^l = \frac{1}{2}n + \frac{1}{4}(2l + 1), LM \right\rangle, \quad (7)$$

where N, n, ν, L, and M are the quantum numbers of $U(N)$, $U(2l + 1)$, $SO(2l + 1)$, $SO(3)$, and $SO(2)$, respectively. κ^l

and μ^l are the quantum numbers of U($2l + 1$) and U(1), respectively. From Eq. (7), it is known that the allowed quantum number n for fixed ν is $n = \nu, \nu + 2, \nu + 4, \ldots$, where ν is called the seniority number [32].

The branching rules for the irreps of the algebra of U(n) → SO(n), which has been discussed by Hamermesh [56], provide the classification of states for the giant dipole spd-IBA model. And pairing models of multilevel configurations are likewise characterized by an overlaid U($n_1 + n_2 + \cdots$) algebraic structure [54], which is

$$\mathrm{U}_{spd}(9) \supset \left\{ \begin{array}{c} \mathrm{SO}_{spd}(9) \\ \mathrm{U}_d(5) \otimes \mathrm{U}_p(3) \otimes \mathrm{U}_s(1) \end{array} \right\}$$
$$\supset \mathrm{SO}_d(5) \otimes \mathrm{SO}_p(3) \supset \mathrm{SO}_d(3)$$
$$\otimes \mathrm{SO}_p(3) \supset \mathrm{SO}_{pd}(3). \quad (8)$$

The operators of infinite-dimensional SU^{spd}(1, 1) algebra [36,39] for GDR are as follows:

$$S_m^\pm(spd) = c_s^{2m+1}S^\pm(s) + c_p^{2m+1}S^\pm(p) + c_d^{2m+1}S^\pm(d) \quad (9)$$

and

$$S_m^0(spd) = c_s^{2m}S^0(s) + c_p^{2m}S^0(p) + c_d^{2m}S^0(d), \quad (10)$$

where c_s, c_p, and c_d are the strengths of the different pairings, and m can be taken to be $0, \pm 1, \pm 2, \ldots$

The lowest-weight states of GDR for SU^{spd}(1, 1) algebra can be defined as

$$|lw\rangle^{spd} = \left| N^{spd}, \kappa_s = \frac{1}{2}\left(\nu_s + \frac{1}{2}\right), \mu_s = \frac{1}{2}\left(n_s + \frac{1}{2}\right), \right.$$
$$\kappa_p = \frac{1}{2}\left(\nu_p + \frac{3}{2}\right), \mu_p = \frac{1}{2}\left(n_p + \frac{3}{2}\right),$$
$$\left. \kappa_d = \frac{1}{2}\left(\nu_d + \frac{5}{2}\right), \mu_d = \frac{1}{2}\left(n_d + \frac{5}{2}\right), L, M \right\rangle, \quad (11)$$

where $N^{spd} = \nu + \nu_p + \nu_s$, $n_d = \nu$, and $n_s = \nu_s = 0$ or 1 for spd-IBA. Then we have

$$S^-(s)|lw\rangle = 0,$$
$$S^-(p)|lw\rangle = 0,$$
$$S^-(d)|lw\rangle = 0,$$
$$S_m^0(spd)|lw\rangle = \Lambda_m^{spd}|lw\rangle, \quad (12)$$

where

$$\Lambda_m^{spd} = c_s^{2m}\frac{1}{2}\left(n_s + \frac{1}{2}\right) + c_p^{2m}\frac{1}{2}\left(n_p + \frac{3}{2}\right) + c_d^{2m}\frac{1}{2}\left(n_d + \frac{5}{2}\right). \quad (13)$$

The interaction of the vector boson with the low-energy s and d modes of the GDR can be introduced into the system in the form a duality relation for the spd Hamiltonian with a number-conserving unitary part and a number-nonconserving quasispin made by using the generators of the SU^{spd}(1, 1) algebra for the transitional region between the two limits. The pairing part of such a model is given as for the sd-IBA. Specifically, the Hamiltonian used to explain the spectral structure of the sd-IBA can be written as

$$\hat{H} = \varepsilon_s n_s + \varepsilon_p n_p + \varepsilon_d n_d - G \sum_{j=s,d} c_j S_j^+ \sum_{j'=s,d} c_{j'} S_{j'}^-$$
$$+ \beta_p \nu_p(\nu_p + 1) + \beta_d \nu_d(\nu_d + 3) + \gamma_p L_p(L_p + 1)$$
$$+ \gamma_d L_d(L_d + 1) + \gamma L(L + 1). \quad (14)$$

Because the energy of the p boson is higher than the energies of the s and d bosons, only the two simplest cases with $n_p = 0$ and $n_p = 1$ are considered in this study, from which it follows that p-boson pairs do not need to be considered, and Eq. (14) can accordingly be reduced to the following:

$$\hat{H} = c_s^2 S_s^0 + c_d^2 S_d^0 - G \sum_{j=s,d} c_j S_j^+ \sum_{j'=s,d} c_{j'} S_{j'}^- + \alpha_p \nu_p$$
$$+ \beta_d \nu_d(\nu_d + 3) + \gamma_d L_d(L_d + 1) + \gamma L(L + 1), \quad (15)$$

where α_p, β_d, γ_d, and γ are real parameters. For simplicity, some of the weak couplings to Casimir operators are not included in this result.

To find the nonzero energy eigenstates with k pairs, we exploit a Fourier-Laurent expansion of the eigenstates. The eigenvectors of the Hamiltonian for excitations can be written as

$$|k; \nu_s \nu_d \nu_p n_\Delta LM\rangle$$
$$= \sum_{n_i \in Z} a_{n_1 n_2 \ldots n_k} x_1^{n_1} x_2^{n_2} x_3^{n_3} \ldots x_k^{n_k} S_{n_1}^+ S_{n_2}^+ S_{n_3}^+ \ldots S_{n_k}^+ |lw\rangle. \quad (16)$$

By using the commutation relations of Eq. (1), it can be verified that all coefficients $a_{n_1 n_2 \ldots n_k}$ in Eq. (16) can be taken to be 1, and then the wave functions can be expressed simply as

$$|k; \nu_s \nu_d \nu_p n_\Delta^s L_s n_\Delta^d L_d n_\Delta^p L_p M\rangle$$
$$= \sum_{n_i \in Z} N' x_1^{n_1} x_2^{n_2} x_3^{n_3} \ldots x_k^{n_k} S_{n_1}^+ S_{n_2}^+ S_{n_3}^+ \ldots S_{n_k}^+ |lw\rangle,$$
$$S_{x_i}^+ = \frac{c_s}{1 - c_s^2 x_i} S^+(s) + \frac{c_d}{1 - c_d^2 x_i} S^+(d) + \frac{c_p}{1 - c_p^2 x_i} S^+(p), \quad (17)$$

where N' is a normalization constant.

In dealing with the seeming complexity of this last expression, a very useful identity known as the BAE [36] can be employed,

$$\frac{\alpha}{x_i} = \sum_{l=0}^{2} \frac{c_l^2 \left(\nu_l + \frac{2l+1}{2}\right)}{1 - c_l^2 x_i} - \sum_{j \neq i} \frac{2}{x_i - x_j}, \quad (18)$$

where ν_s, ν_p, and ν_d are seniority numbers of s, p, and d bosons, respectively. From this, it follows that the eigenvalues $E^{(k)}$ of Hamiltonian Eq. (15) can be written as

$$E^{(k)} = h^{(k)} + \alpha_p \nu_p + \beta_d \nu_d(\nu_d + 3) + \gamma_d L_d(L_d + 1)$$
$$+ \gamma L(L + 1) + \alpha \Lambda_1^l,$$
$$h^{(k)} = \sum_{i=1}^{k} \frac{\alpha}{x_i}. \quad (19)$$

III. NUMERICAL RESULTS

A. Calculation of dipole resonances

In what follows we report on outcomes of our use of the vector boson concept to create excited dipole states and our analyses of various aspects of the associated spectra. The pairing model for the $L_p \otimes L_d$ coupling enables these GDR calculations to be carried out in large configuration spaces. The values of the parameters in the spd-IBA Hamiltonian were determined using least-square-fitting methodologies [36]. Numerical results for negative-parity states of even-even systems with $N = 6$–10 were determined by solving the associated BAEs.

As shown in Refs. [36,57–65], there are many nuclei in the medium-mass region that display spherical to γ-soft phase transition characteristics. Our results for the GDR behavior, calculated for each boson number within the framework of the algebraic sd-IBA, were studied as a function of the pairing strength. The results were then used to analyze the dipole resonance properties of the ground and excited state spectra within the spd framework. In short, we computed the theoretical dipole spectra for the transitional region via Hamiltonian (15). In Table I we list the set of Eq. (15) solutions, which were extracted by solving the BAE for different k pairings with $c_s = [0.1 - 0.63]$ and $c_p = 0$. Due to similar correspondences, we do not present BAE calculations for other pairings.

One of the main challenges is to get the position of the dipole states correct, especially answering the question: What is the position of the lowest 1^- in our calculation? One must keep in mind that it should be lower in energy than the coupling $1 \otimes 0$, where 0 is the ground state's angular momentum in the sd-IBA. For excited states of dipole resonance, we have $L_p \otimes L_d$, where L_p and L_d are the angular momentum of the vector and excited state bosons in the sd-IBA, respectively. In the past we have used the spd-IBA model with up to $1p$ boson to describe dipole-excitation states, as $1p$ boson is enough to get the GDR with the coupling of L_d. In this paper, we have selected L_d's coupling from 0 to 12 to get a far better fix on the GDR. It should be mention that to produce 1^+ states, we need at least $2p$ bosons, but here we only focus on GDR, which is related to 1^- states.

As the examples of our present technique suggest, the level spacing of the GDR, determined within the spd-IBA framework, is given for different boson numbers. Specifically, we have taken 876 level spacings for 1^- states and determined eigenenergies of GDR with $c_s = [0.1$–$0.63]$ with different pairings for all boson numbers from $N = 6$ to $N = 10$. For the sd-IBA parameters we used those given in Ref. [36], but for p-boson parameters, we fit the results to the first experimental $J^p = 1^-$ ground state for each case considered. Specifically we fixed the parameters of the theory using the following input values: $\alpha_p = 885e^{-0.09N}$ keV, $\beta_d = 500e^{-0.78N}$ keV, $\gamma_d = -8.0e^{-0.07N}$ keV, and $\gamma = 23.5e^{-0.16N}$ keV.

Throughout what follows, the three-level pairing model underpins our consideration of GDR excitations. However, the nuclei included in the analysis also exhibit changes from vibrational to γ-soft spectral features as N increases. So while the dipole energy spectra are prominent, the analysis also includes a consideration of the associated spectral statistics.

TABLE I. Solutions of Eq. (15) with $c_s = [0.1$–$0.63]$, $c_p = 0$, $\alpha = 1100$, and $G = 1$.

N	ν_s	ν_d	k	$x_i^\zeta (i = 1, 2, \ldots, k; \zeta = 1, 2, \ldots, k+1)$
6	0	1	2	(1) 99.5016, 99.8388
				(2) 99.7541, 0.996828
				(3) 0.991105, 0.995648
6	1	2	1	(1) 99.3669
				(2) 0.995926
6	0	3	1	(1) 99.5025
				(2) 0.995025
7	1	1	1	(1) 15.9412, 15.9867
				(2) 15.9784, 0.997845
				(3) 0.995648, 0.998348
7	0	2	2	(1) 15.9607, 15.996
				(2) 15.9928, 0.997144
				(3) 0.99777, 0.994746
7	1	3	1	(1) 15.9413
				(2) 0.995023
7	0	4	1	(1) 15.9608
				(2) 0.994124
8	0	1	3	(1) 6.90819, 6.92349, 6.92209
				(2) 6.89071, 6.91405, 0.996826
				(3) 6.89071, 0.995648, 0.998348
				(4) 0.991105, 0.997844, 0.994011
8	1	2	2	(1) 6.89978, 6.91947
				(2) 6.91586, 0.997143
				(3) 0.99291, 0.994745
8	0	3	2	(1) 6.90823, 6.92349
				(2) 6.92209, 0.996426
				(3) 0.991832, 0.991832
8	1	4	1	(1) 6.89983
				(2) 0.994121
8	0	5	1	(1) 6.90827
				(2) 0.993223
9	1	1	3	(1) 4.32433, 4.33668, 4.33442
				(2) 4.3128, 4.32931, 0.996824
				(3) 4.32433, 0.997843, 0.994008
				(4) 0.995646, 0.998347, 0.991102
9	0	2	3	(1) 4.32963, 4.3392, 4.33833
				(2) 4.33329, 4.33953, 0.994745
				(3) 4.33953, 0.989891, 0.99777
				(4) 0.995921, 0.997143, 0.992909
9	1	3	2	(1) 4.32437, 4.33669
				(2) 4.33443, 0.996424
				(3) 0.991827, 0.995017
9	0	4	2	(1) 4.32966, 4.3392
				(2) 4.33833, 0.990765
				(3) 0.995695, 0.994119
9	1	5	1	(1) 4.32441
				(2) 0.993218
10	0	1	4	(1) 2.51335, 2.5189, 2.51839, 2.50699
				(2) 2.51909, 2.51547, 2.5189, 0.99682
				(3) 2.50699, 2.51909, 0.998348, 0.991103
				(4) 2.51335, 0.99682, 0.994005, 0.997842
				(5) 0.991103, 0.998348, 0.995647, 0.99682
10	1	2	3	(1) 2.5103, 2.51745, 2.51614
				(2) 2.50362, 2.51318, 0.995912
				(3) 2.50362, 0.997139, 0.9929
				(4) 0.994741, 0.997768, 0.989884

TABLE I. (*Continued.*)

N	ν_s	ν_d	k	$x_i^\zeta (i = 1, 2, \ldots, k; \zeta = 1, 2, \ldots, k+1)$
10	0	3	3	(1) 2.51337, 2.5189, 2.5184
				(2) 0.507031, 2.51548, 0.996422
				(3) 2.5191, 0.991823, 0.995012
				(4) 0.988704, 0.993844, 0.997167
10	1	4	2	(1) 2.51033, 2.51745
				(2) 2.51615, 0.994106
				(3) 0.987532, 0.992942
10	0	5	2	(1) 2.51339, 2.51891
				(2) 2.5184, 0.99321
				(3) 0.986393, 0.992051
10	1	6	1	(1) 2.51036
				(2) 0.992307

B. Spectral statistics of dipole resonances

To characterize spectral behavior, we use the standard measure of the probability density $P(s)$ of adjacent levels; that is, we use the NNSD (which is the probability of two nearest-neighbor energy levels with the same spin and parity of having a spacing s, see Ref. [66]) as captured by $P(s)$ from the unfolded spectrum. Or stated more simply and succinctly, $P(s)$ is a smoothed approximation to the NNSD that is defined as the energy difference ($s_i = \tilde{E}_{i+1} - \tilde{E}_i$) for two adjacent levels of the same spin and parity.

In the unfolding process, we normalized the average level spacing by $d = \langle s \rangle$, so data with different average level spacing have different chaoticity. As is commonly accepted, the Poisson distribution is defined by

$$P(s) = e^{-s}, \tag{20}$$

which is almost identical to the regular dynamics [4,67,68], while the GOE distribution generically represents the NNSD of systems with Wigner dynamics:

$$P(s) = \tfrac{1}{2}\pi s e^{-\pi s^2/4}. \tag{21}$$

The criteria of chaoticity in energies level distributions is defined in terms of departures from these standard Poisson and Wigner distributions [67–69].

Depending on the details of the chaoticity, some simple distributions have been proposed for describing the spectral statistics of nuclei [70–76] with fewer fitting parameters. For example, in what follows we use the so-called Berry-Robnik distribution (BRD), which interpolates between Poisson statistics with $q = 1$ and GOE with $q = 0$, respectively. In the transition from one limit to another limit for the *spd*-IBA, values of the chaoticity range between 0 and 1 with intermediate statistics showing more or less regular behavior as one departs from the two limits. Specifically, in what follows, our use of BRD is defined as presented in Refs. [71,77]:

$$P(s, q) = \left[q + \tfrac{1}{2}\pi(1-q)s\right]\exp\left[-qs - \tfrac{1}{4}\pi(1-q)s^2\right], \tag{22}$$

which exhibits Poisson and GOE limits by $q = 1$ and 0. (In studying spectral statistics of energy sequences, a comparison of sets of histograms of sequences with the BRD is made to extract a best overall value for q.)

Another distribution that can used to simplify NNSD data is the so-called cumulative distribution [67,69,78]. To further validate and complement our BRD analysis, we have also employed the cumulative distribution, which is defined in terms of the following:

$$I(s) = \int_0^s P(s')ds'. \tag{23}$$

For the Poisson cumulative distribution, we have

$$I_P(s) = 1 - \exp(-s). \tag{24}$$

For the corresponding Wigner cumulative distribution, we have

$$I_W(s) = 1 - \exp(-\pi s^2/4). \tag{25}$$

Our analysis of the statistical properties of the dipole spectrum includes all states from the ground state up to states at 6 MeV. To ensure convergence within this range, the model spaces for states in the separate p space, solved using BAE results, and in the sd spaces, solved using the sd-IBA, had to include all spin and parity states from the BAE results of the sd-IBA ranging from $N = 6$ up to $N = 10$. The total angular momentum of specific states is of course determined by the coupling $L_p \otimes L_d$, where L_p and L_d are the angular momenta of the vector and excited state bosons. The first sets of results are shown in Fig. 1, where we group energy spectra of all boson numbers for $c_p = 0$, 0.3, 0.6, and 0.9 pairing strength.

In what follows, we examine spectra results calculated first in the absence ($c_p = 0$) of vector boson pairing and second in the presence of several selected ($c_p \neq 0$) values of the vector boson pairing. Although the detailed results of these calculations are not included in this paper, the fact that the NNSDs of dipole resonances are strongly dependent upon pairing strength is illustrated through the statistical measures noted above and the results that are provided below. This approach allows us to focus on the statistical properties of the spectra of the dipole states calculated based on the BAE and pairing models as systematically explored across the full 0–6 MeV energy range, which in turn allows us to achieve a more compact and yet comprehensive understanding of the level spacing and spectral features of dipole resonances, which is the primary purpose of this paper.

First, we consider the sd-pairing models c_s and c_d for an even-even system (with different seniority numbers) up to $k = 5$ pairs. The pairing strengths for c_s and c_d are similar to those used in Ref. [36] for the sd-IBM. In the dipole sector, we calculated theoretical dipole states by varying the vector boson c_p pairing strength. Overall, we chose to consider sequences with 220 spacings for each pairing group, including all levels below 6 MeV. In the sd sector, bosons from $N = 6$ to $N = 10$ were included in the analyses.

The value of the chaoticity measure q, as shown in Fig. 1, was deduced from an analysis of the corresponding NNSD. By increasing the c_p values, we obtained a GOE-like distribution around $c_p = 0.6$; specifically, our results show that level statistics obey a GOE distribution in the QPT (critical) region [79]. Changing the values of c_s and c_p between 0 and 1 causes the system to transition from one dynamical symmetry, U(5), to the other, SO(9). The pairing strengths also play
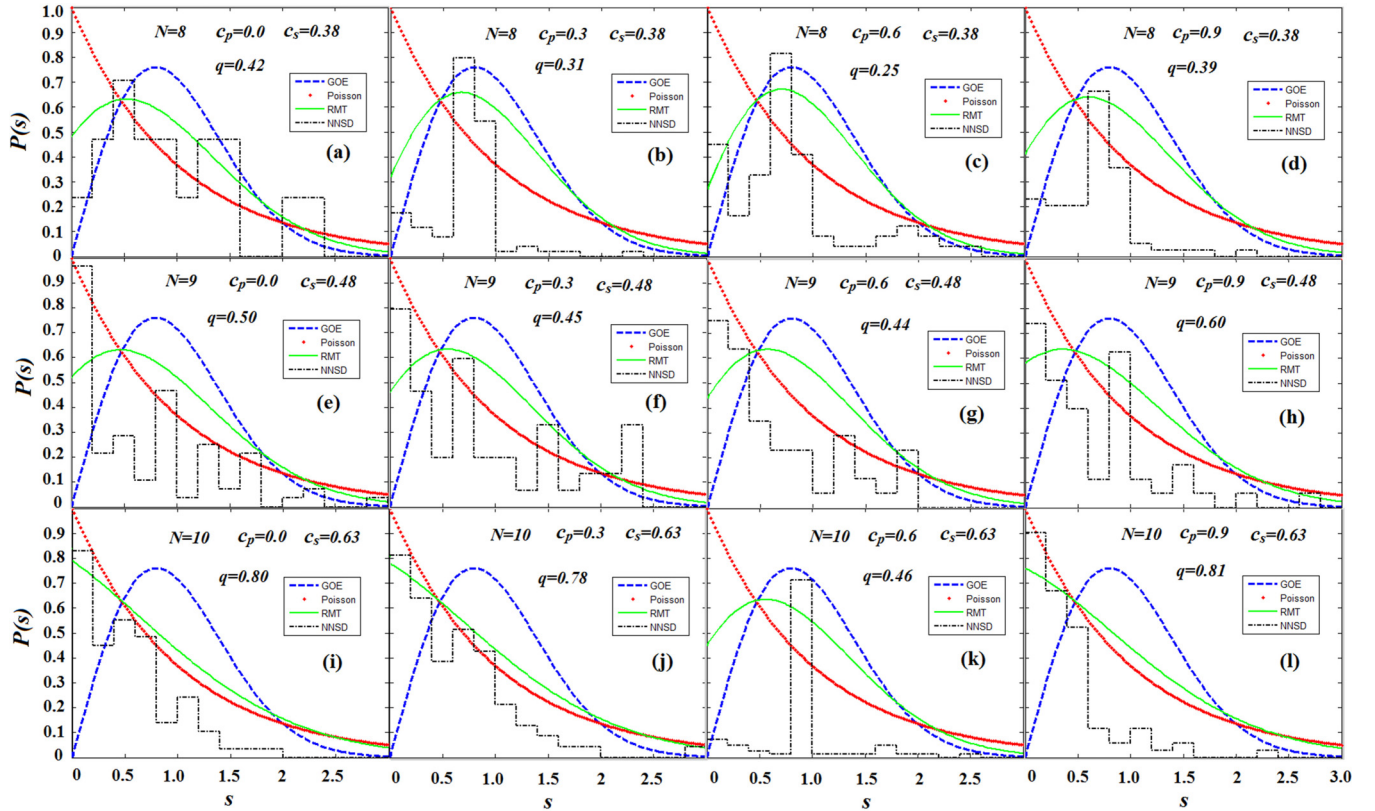
FIG. 1. Spectral statistics of dipole states for different pairing strengths using the RMT and BRD methodologies. Shown are the NNSD of $P(s)$ and histograms obtained from the unfolded energy levels. The green curves show the RMT of the BRD interpolating between regular and chaotic patterns. The parameter q was determined by fitting the GDR results for the NNSD for each level sequence of pairing. We compared the different sequences, and each set of GDRs has converted into a set of normalized spacing. Due to the small number of levels for $N = 6$ and $N = 7$ bosons, they are not shown.

an essential role in determining the position of the dipole resonance. As illustrated in the figures, the $P(s)$ without extra pairing ($c_p = 0$) looks like the sd-IBM spectrum, but with $c_s = 0.1$ and $c_s = 0.63$, $P(s)$ tends to be of the Poisson type. When the model space is expanded to $N = 8$ and $N = 9$, the nearest-neighbor level spacing distribution looks like a GOE distribution. In a complementary alternative analysis, we also examined the effect of pairing correlations on chaoticity by varying vector boson pairing away from 0.3 to 0.6 with the ratios of $c_p/c_s = 0.83$ and 1.25; the nearest-neighbor level spacing distribution $P(s)$ evolved in the direction that is consistent with GOE statistics. When the pairing interaction is even stronger, at around $c_p = 0.9$, a Poisson-type behavior emerges with the ratio of c_s to c_p being $c_p/c_s = 1.42$.

Spectral statistics have been computed for all energy spectra by increasing the pairing strength. Spectral statistics of the dipole states computed by spd-IBA for different pairings are displayed in Figs. 2–5.

The spd-IBA calculations provide interesting results. Near those two limits, the system displays a regular pattern. However, by increasing the pairing strength in the transition region, we observe the onset of chaos, which is compatible with the prediction of Alhassid *et al.* [80,81]. As the number of states for $N = 6$ and $N = 7$ are relatively fewer, we can extend and work out the level number variance up to $N = 10$. The

strongest correlations with three different control parameters for the spd-IBA model are found for $N = 8$ and $N = 9$ nuclei. We can conclude that the coupling between the vector and d-boson components modifies the spectrum, and the NNSD becomes the intermediate surmise.
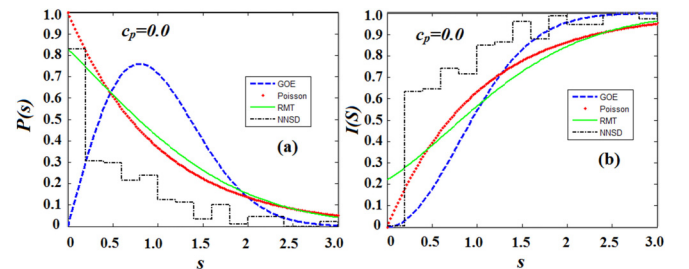

FIG. 2. Spectral statistics of dipole states for different pairing strengths using the RMT and BRD methodologies. Shown are the NNSD of $P(s)$, the integrated NNSD of $I(s)$, and histograms obtained from the unfolded energy levels for $c_p = 0$. The green curves show the RMT of the BRD interpolating between regular and chaotic patterns. Fitting the BRD to the data, we obtain $q = 0.82$. With this strength of pairing, we are near to the dynamical symmetry of the vibrational limit.
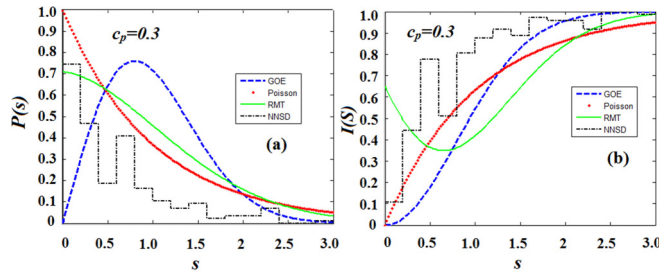
FIG. 3. Spectral statistics of dipole states for different pairing strengths using the RMT and BRD methodologies. Shown are the NNSD of $P(s)$, the integrated NNSD of $I(s)$, and histograms obtained from the unfolded energy levels for $c_p = 0.3$. The green curves show the RMT of the BRD interpolating between regular and chaotic patterns. Fitting the BRD to the data, we obtain $q = 0.70$. With this strength of pairing, we are in the transition region of the vibrational and γ-soft limits.

The nuclear dipole states are well separated, like those of $c_p = 0.0$ and $c_p = 0.9$ in the average level spacings $\langle d \rangle \approx$ 248.8 and 154.2 keV, respectively. In comparison with well-separated levels, illustrated by the closely spaced levels for the $c_p = 0.3$ and $c_p = 0.6$ pairing, the average level spacings are $\langle d \rangle \approx 111.7$ and 16.7 keV, respectively. We have learned that in the transition region for closely spaced levels of $\langle d \rangle \approx 16.7$, neighboring states contain information about the chaoticity, and the spectrum for this region is chaotic. These properties and trends are consistent with the nuclear system's chaoticity in closely spaced levels [82] that may cause strongly mixed wave functions and modify the nuclear structure of many-body systems [83–85]. These neighboring states with strongly mixed wave functions with the same spin and parity are prevalent in the closely spaced levels.

Now we group neighboring states with the same angular momentum quantum numbers. If we group levels with the symmetry representation's angular momentum contents, the neighboring levels of coupling $(L_p \bigotimes L_d)$ belong to different classes. Under this condition, we expect the NNSD sequence of level spacings to be similar to the GOE distribution. This
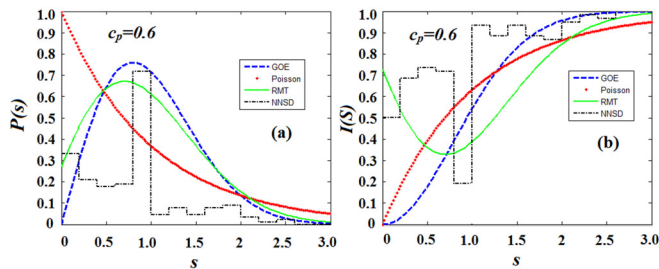
distribution reveals some short-range order levels as well as significant gaps. In the neighboring states with the same quantum numbers cases, when we have a coupling group for all sets of pairings, one can see the onset of spectral chaos at excitation energy (see Fig. 6). These energy spectra belong to all $c_p = 0, 0.3, 0.6,$ and 0.9 pairing strengths.
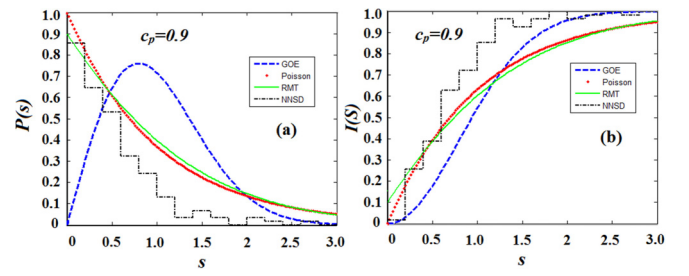

FIG. 5. Spectral statistics of dipole states for different pairing strengths using the RMT and BRD methodologies. Shown are the NNSD of $P(s)$, the integrated NNSD of $I(s)$, and histograms obtained from the unfolded energy levels for $c_p = 0.9$. The green curves show the RMT of BRD interpolating between regular and chaotic patterns. Fitting the BRD to the data, we obtain $q = 0.88$. With this strength of pairing, we are near to the dynamical symmetry of the γ-soft limit.

FIG. 4. Spectral statistics of the dipole states computed by *spd*-IBA. Shown are the NNSD of $P(s)$ and the integrated NNSD of $I(s)$. Histograms were obtained from the unfolded energy levels for the pairing of $c_p = 0.6$, and the green curves show the RMT of BRD interpolating between regular and chaotic patterns. Fitting the BRD to the data, we obtain values for $q = 0.26$. With this strength of pairing, we are in the transition region of vibrational and γ-soft limits.
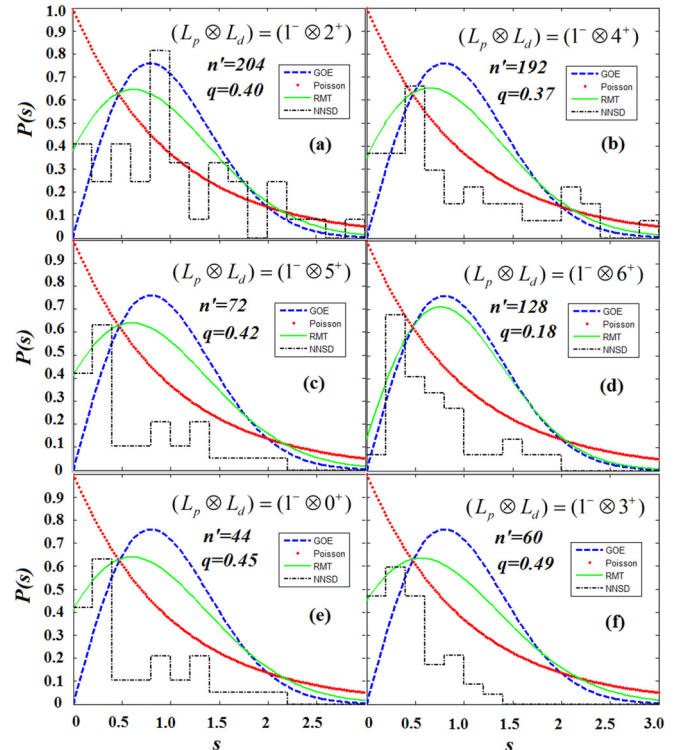

FIG. 6. Spectral statistics of the neighboring levels of coupling $(L_p \bigotimes L_d)$. They are compared to the Poisson (red line) and the GOE (blue line) distributions. Histograms were obtained from the unfolded energy levels for all pairings. The corresponding values of the chaoticity parameter q and the number of level spacing n' are given for each coupling. Due to similar correspondences, we do not present the level statistics for those with larger L_d couplings.

The optimal probability of our distribution result is formulated in terms of a Cramer-Rao lower bound (CRLB) minimization problem [86]. One of the first aims of estimation theory is the expansion of bounds on the most feasible operation. Such bounds prepare criteria against which we can correlate the carrying out of any proposed estimator. This criterion is the Cramer-Rao bound, which denotes the smallest possible total variance of chaoticity, i.e., an estimator of q. The CRLB is a method for obtaining the accuracy of the estimator parameters. If the estimator is a minimum variance estimator, then its parameter variance achieves the lower bound, that is, the Cramer-Rao bound. Thus, to further decrease the variance of the minimum variance estimator, one can only optimize the distribution so that the corresponding Cramer-Rao bound is decreased. We have to minimize the errors by CRLB. First, we introduce the Fisher information $F(q)$, and this Fisher information is defined as an optimization problem:

$$F(q) = E\left[\left(\frac{\partial \ln P(s; q)}{\partial q}\right)^2\right], \qquad (26)$$

where a system in which a quantized version of the observation s is used to estimate an underlying parameter q and E denotes the expected value (over s). As the estimation of the CRLB is the inverse of $F(q)$, the variance of the estimator is defined as follows:

$$\mathrm{var}(q) \geqslant \frac{1}{MF(q)}, \qquad (27)$$

where M is the sample size. By calculating $F(q)$, the scalar quantity $\frac{1}{MF(q)}$ is the CRLB on the variances of unbiased estimators. The minimum CRLB corresponds to the final value in the iteration procedure. The Newton-Raphson procedure can be used to approximate the solution q, giving an approximation to the CRLB. This algorithm converges to the exact solution q in τ iterations. The variance estimates of the estimators are obtained by repeating the Newton-Raphson procedure for $\tau = 1000$ to get the minimum variance for the CRLB. The process is repeated until a sufficiently precise value is reached. However, when carried to termination, it is not computationally competitive with the least square fitting. We have used the least square fitting results as an initial guess for a root of distribution in iterative root-finding procedures.

Finally, to find the efficiencies of considered distribution via fitting, we determined the CRLB, the right-hand side of the Cramer-Rao inequality (27), as $\mathrm{CRLB} \equiv \frac{1}{MF(q)}$. For the final value, q is obtained from fitting processes. We have evaluated the NNSD for different pairings. To compare the efficiencies of the BRD in different sequences of dipole resonance by the iteration processes, we have calculated the CRLB for different pairing strengths of c_p where $c_s = 0.1$ and $c_p = 0$ have the lowest CRLB by comparison with other pairing strengths. The variations of CRLBs in the iteration processes for different pairing strengths of c_p are displayed in Fig. 7.

To get further insight into the nature of GDRs in the medium-mass region, we also inspected the sequences of the NNSD for the 342 states with $J^p = 1^-$ and for the 97 states with $J^p = 1^+$. In addition to the references cited herein for the pygmy and giant dipole resonances, several workers
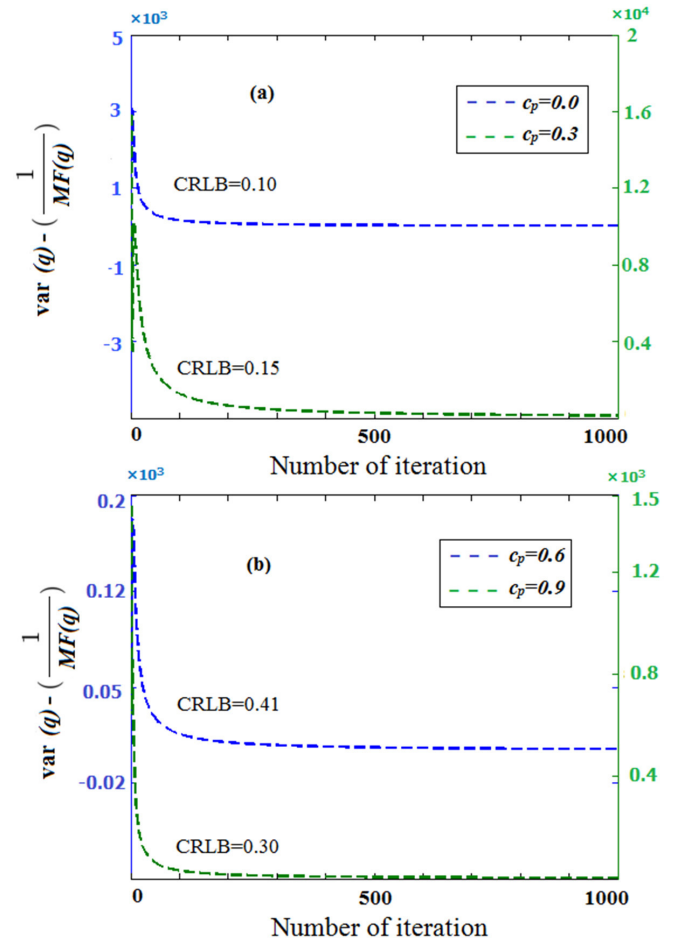

FIG. 7. The variations of CRLBs in the iteration processes for different pairing strengths of c_p.

TABLE II. A description of the available data of dipole negative-parity states in the analysis. M describes the number of selected levels and E_i and E_f represent the lowest and the highest levels contributed to each nucleus.

Nuclei	M	E_i (keV)	E_f (keV)	Reference
^{32}S	5	7480	11710	[87]
^{40}Ca	5	6612.2	9545.7	[88]
^{52}Cr	20	5098.6	9236.6	[89]
^{56}Fe	9	6925.4	9287.6	[90]
^{58}Ni	11	7048.2	9723.0	[90]
^{60}Ni	48	6180.6	9892.6	[91]
^{70}Ge	11	4356.6	7753.0	[92]
^{72}Ge	7	5849.5	8441.2	[92]
^{74}Ge	11	4224.9	7652.1	[92]
^{76}Ge	12	5698.9	9013.2	[92]
^{76}Se	76	4601.6	7093.1	[93]
^{86}Kr	23	4867.4	9085.6	[94]
^{88}Sr	48	4742.7	10644.1	[95]
^{90}Zr	15	6295.8	10042.9	[96]
^{116}Sn	32	4547.1	8361.3	[97]
^{124}Sn	35	5842.5	8376.2	[97]
^{138}Ba	9	4025.2	6102.7	[98]

TABLE III. A description of the available data of dipole positive-parity state in the analysis. M describes the number of selected levels and E_i and E_f represent the lowest and the highest levels contributed to each nucleus.

Nuclei	M	E_i (keV)	E_f (keV)	Reference
^{50}Cr	15	3628.2	9719.1	[99]
^{52}Cr	25	5098.6	9429.0	[89]
^{56}Fe	7	3448.6	8908.9	[90]
^{58}Ni	8	5905.3	9156.9	[90]
^{60}Ni	32	3193.6	9830	[91]
^{74}Ge	6	3093.4 5	6733.4	[100]
^{76}Se	11	4055.2	7110.1	[93]

FIG. 9. Spectral statistics of the experimental dipole states $J^p = 1^+$. Shown are the NNSD of $P(s)$ and the integrated NNSD of $I(s)$. Histograms were obtained from the unfolded energy levels for the $J^p = 1^+$ states. Fitting the BRD to the data, we obtain $q = 0.87$.

have investigated experimental features in somewhat light- and medium-mass nuclei. These include from ^{32}S to ^{138}Ba [87–100]. The lowest and highest experimental dipole states with the number of selected levels are listed in Tables II and III.

The calculated chaoticity values together with the NNSD displayed in Figs. 8 and 9 reveal some regularity in dipole resonances. We analyzed the NNSD for the positive $J^p = 1^+$ and negative $J^p = 1^-$ parity states to clarify the chaotic and regular spectral properties of validated GDR. For these modes, we find a tendency towards Poisson behavior. Our *spd*-IBA and spectral statistics calculations facilitate a satisfactory description of the GDR's properties in the proposed nuclei. All ground and excited states are included in the calculation of the NNSD. Again, variations of CRLBs are shown in Fig. 10 for experimental $J^p = 1^-$ and $J^p = 1^+$ states. In the variations of CRLBs curves, the meaning of the scales on the vertical axis is that it allows the assessment of how close a given estimation method is to optimality. In particular, if the variance of an unbiased estimate is equal to the Cramer-Rao bound, then it has minimum variance. The estimated parameters display a reduction of uncertainties and yield estimator's variances very close to CRLBs, as shown in Figs. 7 and 10. This means that the difference between the left and right sides of Eq. (27) can be used to describe the variation (decreasing) of uncertainties for estimated parameters during the iterations. From these curves, it is obvious that the CRLB serves as a good approx-
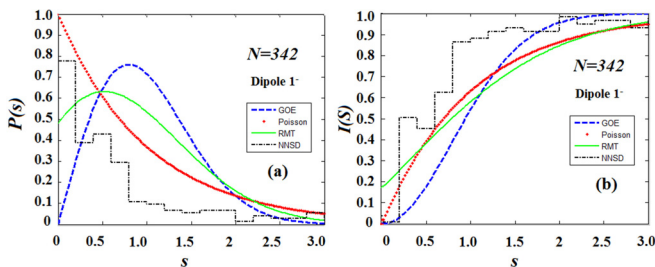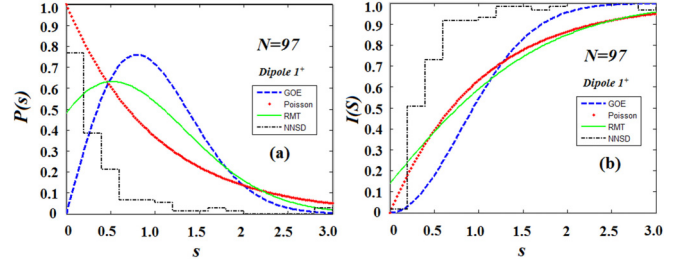
imation to the estimator's variance, particularly for spherical symmetry with $c_p = 0$.

We have seen from the estimated values of the BRD parameter q shown in Figs. 8 and 9 that level energies near dynamical U(5) and SO(9) symmetries in the *spd*-IBA model seem more regular. Similar to the predictions made by Enders in Ref. [101], the spectra of medium-mass nuclei for dipole states seem almost regular, while for the predictions in light nuclei made by Dietz in Ref. [70], the spectra for negative- and positive-parity states are almost regular and chaotic, respectively. It has been verified that the NNSD is governed by the interplay between the GDR and the pairing interaction for BAE calculated from the *spd*-IBA model. From theory, based on the spectral statistics for most spectra in the *spd*-IBA model around dynamical symmetries, vibrational and γ-soft, the NNSDs for dipole states show behavior similar to that of experiments.

Finally, we conclude that a phenomenological collective model for the IBA is the best tool to investigate the spectra for dipole states. This collective model estimates dipole resonances to calculate the level spacing distribution with the pairing model. In addition to its consistency, our *spd*-IBA model in GDR is computationally so simple that it can be

FIG. 8. Spectral statistics of the experimental dipole states $J^p = 1^-$. Shown are the NNSD of $P(s)$ and the integrated NNSD of $I(s)$. Histograms obtained from the unfolded energy levels for the $J^p = 1^-$ states. Fitting the BRD to the data, we obtain $q = 0.81$.
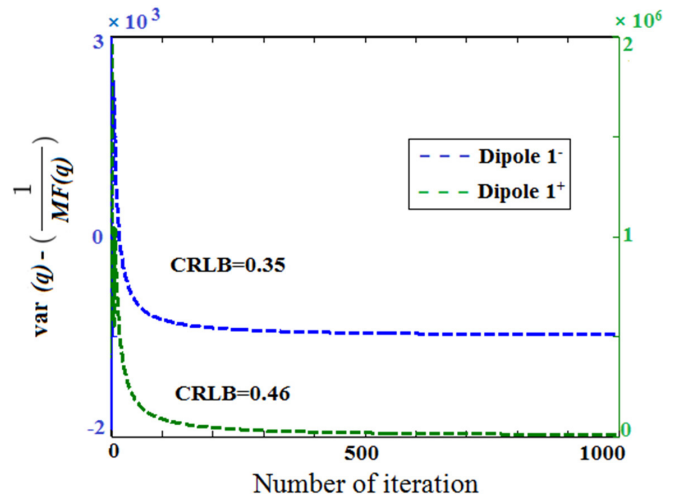

FIG. 10. The variations of CRLBs in the iteration processes for dipole $J^p = 1^-$ and $J^p = 1^+$ states.

easily applied to large sets of collective models, such as *sdg*- and *sdf*-IBA.

IV. SUMMARY AND CONCLUSION

We conclude that the *spd*-IBA can reproduce dipole states in a wide variety of nuclei. The proposed model and properties of the GDRs are investigated in medium-mass nuclei ($E \leqslant 12$ MeV). It has been demonstrated that the *spd*-IBA is a quite powerful tool to investigate nuclear structures. In this paper, We have studied the GDRs within an extended pairing model with a focus on spectral statistics. The next case is the energy spectra that have been analyzed using both the *spd*-IBA and the BAE. The effect of pairing correlations on spectral statistics is the primary result of this paper. We have found that varying the pairing interaction strength for vector boson c_p is likely to alter the statistical properties of the spectra. The *spd*-IBA undergoes vibrational to γ-unstable shape phase transition. We have seen that the dipole spec- trum obeyed GOE statistics for boson numbers, which were near the critical point. In contrast, the spectra become regular for those nuclei near either vibrational or γ-unstable points. Because of the appropriate success of the *spd*-IBA in chaos and regularity of nuclei, the investigation of another extension of the IBA in *sdf*-, *sdg*-, and *spdf*-boson systems should be feasible.

[1] J. M. G. Gómez, K. Kar, V. K. B. Kota, R. A. Molina, A. Relaño, and J. Retamosa, Phys. Rep. **499**, 103 (2011).

[2] A. P. Severyukhin, S. Åberg, N. N. Arsenyev, and R. G. Nazmitdinov, Phys. Rev. C **98**, 044319 (2018).

[3] A. Magner, A. Levon, and S. Radionov, Eur. Phys. J. A **54**, 214 (2018).

[4] H. A. Weidenmüller and G. E. Mitchell, Rev. Mod. Phys. **81**, 539 (2009).

[5] V. Zelevinsky, B. A. Brown, N. Frazier, and M. Horoi, Phys. Rep. **276**, 85 (1996).

[6] G. Maino, A. Ventura, L. Zuffi, and I. Iachello, Phys. Rev. C **30**, 2101 (1984).

[7] D. Kusnezov and W. E. Ormand, Phys. Rev. Lett. **90**, 042501 (2003).

[8] D. J. Rowe and F. Iachello, Phys. Lett. B **130**, 231 (1983).

[9] H. Emling, Prog. Part. Nucl. Phys. **33**, 729 (1994).

[10] Ph. Chomaz and N. Frascaria, Phys. Rep. **252**, 275 (1995).

[11] P. Ring and P. Schuck, *The Nuclear Many-Body Problem* (Springer, Heidelberg, 1980).

[12] X. Roca-Maza, G. Pozzi, M. Brenna, K. Mizuyama, and G. Colò, Phys. Rev. C **85**, 024601 (2012).

[13] H. Hergert, P. Papakonstantinou, and R. Roth, Phys. Rev. C **83**, 064317 (2011).

[14] F. G. Scholtz, Phys. Lett. B **151**, 87 (1985).

[15] F. G. Scholtz and F. J. W. Hahne, Phys. Rev. C **34**, 693 (1986).

[16] I. Morrison and J. Weise, J. Phys. G: Nucl. Phys. **8**, 687 (1982).

[17] G. Maino, A. Ventura, and L. Zuffi, Phys. Rev. C **37**, 1379 (1988).

[18] M. V. Andres *et al.*, Phys. Lett. B **470**, 6 (1999).

[19] C. E. Alonso *et al.*, Nucl. Phys. A **679**, 359 (2001).

[20] S. D. Hoblit and A. M. Nathan, Phys. Rev. C **44**, 2372 (1991).

[21] F. G. Scholtz and F. J. W. Hahne, Phys. Lett. B **123**, 147 (1983).

[22] F. Iachello, Phys. Lett. B **160**, 1 (1985).

[23] G. Maino, A. Ventura, P. Van Isacker, and L. Zuffi, Phys. Rev. C **33**, 1089 (1986).

[24] F. G. Scholtz and F. J. W. Hahne, Nucl. Phys. A **471**, 545 (1987).

[25] G. Maino, Phys. Rev. C **40**, 988 (1989).

[26] S. Turrini, G. Maino, and A. Ventura, Phys. Rev. C **39**, 824 (1989).

[27] G. Maino, A. Ventura, and L. Zuffi, Phys. Rev. C **46**, 1725 (1992).

[28] A. Arima and F. Iachello, Phys. Rev. Lett. **35**, 1069 (1975).

[29] A. Arima and F. Iachello, Ann. Phys. **99**, 253 (1976).

[30] A. Arima and F. Iachello, Ann. Phys. **111**, 201 (1978).

[31] A. J. Majarshin and H. Sabri, Nucl. Phys. A **964**, 69 (2017).

[32] F. Iachello and A. Arima, *The Interacting Boson Model* (Cambridge University, Cambridge, England, 1987).

[33] O. Scholten, F. Iachello, and A. Arima, Ann. Phys. **115**, 325 (1978).

[34] A. Arima and F. Iachello, Ann. Phys. **123**, 468 (1979).

[35] F. Iachello, Phys. Rev. Lett. **85**, 3580 (2000).

[36] F. Pan and J. Draayer, Nucl. Phys. A **636**, 156 (1998).

[37] F. Pan and J. P. Draayer, Phys. Lett. B **442**, 7 (1998).

[38] F. Pan and J. P. Draayer, Ann. Phys. **275**, 224 (1999).

[39] F. Pan, X. Zhang, and J. Draayer, J. Phys. A: Math. Gen. **35**, 7173 (2002).

[40] F. Pan, V. G. Gueorguiev, and J. P. Draayer, Phys. Rev. Lett. **92**, 112503 (2004).

[41] F. Pan *et al.*, Phys. Lett. A **341**, 291 (2005).

[42] F. Pan, Y. Zhang, H.-C. Xu, L.-R. Dai, and J. P. Draayer, Phys. Rev. C **91**, 034305 (2015).

[43] M. A. Jafarizadeh, A. J. Majarshin, and N. Fouladi, Int. J. Mod. Phys. E **25**, 1650089 (2016).

[44] A. J. Majarshin and M. A. Jafarizadeh, Nucl. Phys. A **968**, 287 (2017).

[45] A. J. Majarshin, M. A. Jafarizadeh, and H. Sabri, Eur. Phys. J. Plus **132**, 418 (2017).

[46] M. A. Jafarizadeh *et al.*, J. Phys. G: Nucl. Part. Phys. **43**, 095108 (2016).

[47] R. W. Richardson, Phys. Lett. **3**, 277 (1963).

[48] R. W. Richardson and N. Sherman, Nucl. Phys. **52**, 221 (1964).

[49] F. Pan, J. P. Draayer, and W. E. Ormand, Phys. Lett. B **422**, 1 (1998).

[50] J. Dukelsky, C. Esebbag, and P. Schuck, Phys. Rev. Lett. **87**, 066403 (2001).

[51] A. J. Majarshin, Eur. Phys. J. A **54**, 11 (2018).

[52] A. J. Majarshin, H. Sabri, and M. A. Jafarizadeh, Eur. Phys. J. A **54**, 1 (2018).

[53] A. J. Majarshin *et al.*, Chin. Phys. C **45**, 2 (2021).

[54] M. Caprio, P. Cejnar, and F. Iachello, Ann. Phys. **323**, 1106 (2008).

[55] D. J. Rowe, M. J. Carvalho, and J. Repka, Rev. Mod. Phys. **84**, 711 (2012).

[56] M. Hamermesh, *Group Theory and its Application to Physical Problems* (Courier Corporation, New York, 2012).

[57] A. Frank, C. E. Alonso, and J. M. Arias, Phys. Rev. C **65**, 014301 (2001).

[58] R. M. Clark, M. Cromaz, M. A. Deleplanque, M. Descovich, R. M. Diamond, P. Fallon, I. Y. Lee, A. O. Macchiavelli, H. Mahmud, E. Rodriguez-Vieitez, F. S. Stephens, and D. Ward, Phys. Rev. C **69**, 064322 (2004).

[59] P. Van Isacker and G. Puddu, Nucl. Phys. A **348**, 125 (1980).

[60] M. Buyokata, P. Van Isacker, and I. Uluer, J. Phys. G: Nucl. Part. Phys. **37**, 105102 (2010).

[61] X. F. Meng, F.-r. Wang, Y.-a. Luo, F. Pan, and J. P. Draayer, Phys. Rev. C **77**, 047304 (2008).

[62] N. V. Zamfir *et al.*, Phys. Rev. C **65**, 044325 (2002).

[63] J. Kern *et al.*, Nucl. Phys. A **593**, 21 (1995).

[64] S. F. Hicks, J. C. Boehringer, N. Boukharouba,C. Fransen,S. R. Lesher, J. M. Mueller, J. R. Vanhoy, and S. W. Yates, Phys. Rev. C **86**, 054308 (2012).

[65] K. Nomura, R. Rodríguez-Guzmán, and L. M. Robledo, Phys. Rev. C **94**, 044314 (2016).

[66] A. J. Majarshin *et al.* Phys. Scr. **95**, 105305 (2020).

[67] A. I. Levon, A. G. Magner, and S. V. Radionov, Phys. Rev. C **97**, 044305 (2018).

[68] A. Y. Abul-Magd, H. L. Harney, M. H. Simbel, and H. A. Weidenmüller, Phys. Lett. B **579**, 278 (2004).

[69] B. Dietz, A. Heusler, K. H. Maier, A. Richter, and B. A. Brown, Phys. Rev. Lett. **118**, 012501 (2017).

[70] B. Dietz, B. A. Brown, U. Gayer, N. Pietralla, V. Y. Ponomarev, A. Richter, P. C. Ries, and V. Werner, Phys. Rev. C **98**, 054314 (2018).

[71] A. J. Majarshin, F. Pan, H. Sabri, and J. P. Draayer, Ann. Phys. **407**, 250 (2019).

[72] M. V. Berry and M. Robnik, J. Phys. A: Math. Gen. **17**, 2413 (1984).

[73] M. C. Gutzwiller, *Chaos in Classical and Quantum Mechanics* (Springer, New York, 2013).

[74] M. S. Bae, T. Otsuka, T. Mizusaki, and N. Fukunishi, Phys. Rev. Lett. **69**, 2349 (1992).

[75] K. Roy, B. Chakrabarti, N. Chavda, V. Kota, M. Lekala, and G. Rampho, Europhys. Lett. **118**, 46003 (2017).

[76] P. Fanto, Y. Alhassid, and H. A. Weidenmüller, Phys. Rev. C **101**, 014607 (2020).

[77] C. Fang-Qi, S. Yang, and Z. Xian-Rong, Chin. Phys. C **33**, 24 (2009).

[78] L. Muñoz, R. A. Molina, J. M. G. Gómez, and A. Heusler, Phys. Rev. C **95**, 014317 (2017).

[79] H. Wu and M. Valliéres, J. Phys. G: Nucl. Part. Phys. **16**, L149 (1990).

[80] Y. Alhassid, A. Novoselsky, and N. Whelan, Phys. Rev. Lett. **65**, 2971 (1990).

[81] Y. Alhassid and A. Novoselsky, Phys. Rev. C **45**, 1677 (1992).

[82] J. D. Garrett, J. Q. Robinson, A. J. Foglia, and H. Q. Jin, Phys. Lett. B **392**, 24 (1997).

[83] L. Dai, F. Pan, Z. Feng, Y. Zhang, S. Cui, and J. Draayer, Chin. Phys. C **44**, 064102 (2020).

[84] A. J. Majarshin, Y.-A. Luo, F. Pan, H. T. Fortune, and J. P. Draayer, Phys. Rev. C **103**, 024317 (2021).

[85] A. J. Majarshin, Y.-A. Luo, F. Pan, and H. T. Fortune, Phys. Rev. C **104**, 014321 (2021).

[86] S. K. Rao, in *Conference Record of Thirty-Second Asilomar Conference on Signals, Systems and Computers* (Cat. No. 98CH36284) (IEEE, New York, 1998), p. 441.

[87] M. Itoh *et al.*, Phys. Rev. C **88**, 064313 (2013).

[88] T. Hartmann, J. Enders, P. Mohr, K. Vogt, S. Volz, and A. Zilges, Phys. Rev. C **65**, 034301 (2002).

[89] H. Pai *et al.*, Phys. Rev. C **88**, 054316 (2013).

[90] F. Bauwens *et al.*, Phys. Rev. C **62**, 024302 (2000).

[91] M. Scheck *et al.*, Phys. Rev. C **88**, 044304 (2013).

[92] A. Jung *et al.*, Nucl. Phys. A **584**, 103 (1995).

[93] P. Goddard *et al.*, Phys. Rev. C **88**, 064308 (2013).

[94] R. Schwengner *et al.*, Phys. Rev. C **87**, 024306 (2013).

[95] R. Schwengner *et al.*, Phys. Rev. C **76**, 034321 (2007).

[96] R. Schwengner *et al.*, Phys. Rev. C **78**, 064314 (2008).

[97] K. Govaert, F. Bauwens, J. Bryssinck, D. De Frenne, E. Jacobs, W. Mondelaers, L. Govor, and V. Y. Ponomarev, Phys. Rev. C **57**, 2229 (1998).

[98] R.-D. Herzberg, C. Fransen, P. von Brentano, J. Eberth, J. Enders, A. Fitzler, l. Kaubler, H. Kaiser, P. von Neumann-Cosel, N. Pietralla, V. Y. Ponomarev, H. Prade, A. Richter, H. Schnare, R. Schwengner, S. Skoda, H. G. Thomas, H. Tiesler, D. Weisshaar, and I. Wiedenhover, Phys. Rev. C **60**, 051307(R) (1999).

[99] H. Pai *et al.*, Phys. Rev. C **93**, 014318 (2016).

[100] R. Massarczyk *et al.*, Phys. Rev. C **92**, 044309 (2015).

[101] J. Enders, T. Guhr, A. Heine, P. von Neumann-Cosel, V. Y. Ponomarev, A. Richter, and J. Wambach, Nucl. Phys. A **741**, 3 (2004).